Ion Selectivity of Crown Ethers Investigated by UV and IR Spectroscopy in a Cold Ion Trap

Yoshiya Inokuchi,[‡,*] Oleg V. Boyarkin,[†] Ryoji Kusaka,[‡] Takeharu Haino,[‡] Takayuki Ebata,[‡] and Thomas R. Rizzo[†,*]

Department of Chemistry, Graduate School of Science, Hiroshima University, Higashi-Hiroshima, Hiroshima 739-8526, Japan and Laboratoire de Chimie Physique Moléculaire, École Polytechnique Fédérale de Lausanne, Lausanne CH-1015, Switzerland

E-mail: y-inokuchi@hiroshima-u.ac.jp (YI), thomas.rizzo@epfl.ch (TRR)

Abstract

Electronic and vibrational spectra of benzo-15-crown-5 (B15C5) and benzo-18-crown-6 (B18C6) complexes with alkali metal ions, M^+•B15C5 and M^+•B18C6 (M = Li, Na, K, Rb and Cs), are measured using UV photodissociation (UVPD) and IR-UV double resonance spectroscopy in a cold, 22-pole ion trap. We determine the structure of conformers with the aid of density functional theory calculations. In the Na^+•B15C5 and K^+•B18C6 complexes, the crown ethers open the most and hold the metal ions at the center of the ether ring, demonstrating the optimum matching in size between the cavity of the crown ethers and the metal ions. For smaller ions, the crown ethers deform the ether ring to decrease the distance and increase the interaction between the metal ions and oxygen atoms; the metal ions are completely surrounded by the ether ring. In the case of larger ions, the metal ions are

too large to enter the crown cavity and are positioned on it, leaving one of its sides open for further solvation. Thermochemistry data calculated on the basis of the stable conformers of the complexes suggest that the ion selectivity of crown ethers is controlled primarily by the enthalpy change for the complex formation in solution, which depends strongly on the complex structure.

Keywords: alkali metal ions, 18-crown-6, 15-crown-5, encapsulation

*To whom correspondence should be addressed.

[‡]Hiroshima University

[†]École Polytechnique Fédérale de Lausanne

1. Introduction

One remarkable characteristic of crown ethers is their high selectivity in encapsulating guest species such as metal ions. After the discovery of crown ethers by Pedersen,[1,2] considerable effort was made to understand their selectivity in solution by measuring thermodynamic and kinetic data such as equilibrium constants, enthalpy and entropy changes (ΔH and ΔS), and rate constants.[3] Their ability for preferential encapsulation has been explained mainly in terms of size matching between crown ethers and guest species.[3] For instance, 18-crown-6 (18C6) and 15-crown-5 (15C5) selectively capture K^+ and Na^+ ions, respectively, among alkali metal ions,[3] although it was not necessarily the case that the complex structure was fully elucidated. While the structure of metal ion–crown ether complexes has been extensively examined by X-ray diffraction analysis,[4] in crystals counter anions coordinate to metal cations, which causes substantial change of the complex structure from that in solution. Metal ion–crown ether complexes have also been extensively investigated in the gas phase by mass spectrometric[5–17] and ion mobility methods.[18,19] The binding energy of 18C6 with alkali metal ions shows a maximum value for Li^+, which is not consistent with the selective capture of K^+. More recently, the structures of metal ion–crown ether complexes have been investigated in the gas phase by both IR[20–27] and UV spectroscopy.[28–30] We have reported highly resolved UV and IR spectra of dibenzo-18-crown-6 (DB18C6) complexes with alkali metal ions in a cooled, 22-pole ion trap.[31] The M^+•DB18C6 (M = Li, Na, K, Rb and Cs) complexes show many well-resolved vibronic bands in the UV spectra, which enable us to determine the number and the structure of conformers. Our goal is to examine the structure of metal ion–crown ether complexes in the gas phase by UV and IR spectroscopy to more fully understand the origin of the selectivity of crown ethers for ion capture.

In the present work, we investigate the conformation of cold complexes of benzo-15-crown-5 (B15C5) and benzo-18-crown-6 (B18C6) (Scheme 1) with alkali metal ions, M^+•B15C5 and M^+•B18C6 (M = Li, Na, K, Rb and Cs). The M^+•B15C5 and M^+•B18C6 complexes are produced by nanoelectrospray, mass-selected by a quadrupole mass spectrometer and irradiated with a UV laser in a cold, 22-pole ion trap, where the complexes are cooled down to ~10 K.[32,33] Isolating and cooling the complexes in the gas phase greatly simplify the UV spectra and provide well-resolved vibronic bands. Furthermore, we measure conformer-specific infrared spectra *via* IR-UV double resonance in the CH stretching (2800–3120 cm^{-1}) region. Although the observed IR spectra are more congested than predicted by quantum chemical calculations because of Fermi resonance interactions, we can still use these spectra to distinguish peaks in the UV spectra that belong to different conformers. The use of density functional theory (DFT) and time-dependent DFT (TD-DFT) allows us to determine the conformation of the complexes. We finally discuss the relation between the complex structure in the gas phase and the ion selectivity in solution.

2. Experimental and computational methods

The details of our experimental approach have been given elsewhere.[31, 34] Briefly, the M^+•B15C5 and M^+•B18C6 (M = Li, Na, K, Rb and Cs) complexes are produced continuously at atmospheric pressure *via* nanoelectrospray, mass-selected in a quadrupole mass filter and injected into a 22-pole RF ion trap, which is cooled by a closed cycle He refrigerator to 4 K. The trapped ions are cooled internally and translationally to ~10 K through collisions with cold He buffer gas,[31–34] which is pulsed into the trap. The trapped ions are then irradiated with a UV laser pulse, which causes some fraction of them to dissociate. The resulting charged photofragments, as well as the remaining parent ions, are released from the trap, mass-analyzed by a quadrupole

mass filter and detected with a channeltron electron multiplier. Ultraviolet photodissociation (UVPD) spectra of parent ions are obtained by plotting the yield of a particular photofragment ion as a function of the wavenumber of the UV laser. For IR-UV double resonance spectroscopy, the output pulse of an IR OPO counter-propagates collinearly with the UV pulse, arriving in the trap ~100 ns prior to it. The wavenumber of the UV laser is fixed to a particular vibronic band in the electronic spectra for monitoring the population of a conformer and the wavenumber of the OPO is scanned while monitoring fragment ion intensity induced by the UV laser. Conformer-specific IR spectra are obtained by plotting the yield of a particular photofragment as a function of the OPO wavenumber. For distinguishing vibronic bands due to different conformers, we measure UVPD spectra with the OPO wavenumber fixed to a particular vibrational band.

For geometry optimization of the M^+•B15C5 and M^+•B18C6 complexes, we first use a classical force field to find conformational minima. The initial conformational search is performed by using the mixed torsional search with low-mode sampling and the MMFF94s force field as implemented in MacroModel V. 9.1.[35] Minimum-energy conformers found with the force field calculations are then optimized at the M05-2X/6-31+G(d) level with *loose* optimization criteria with the GAUSSIAN09 program package.[36] Unique minima obtained by comparison of relative energies and rotational constants are further optimized at the M05-2X/6-31+G(d) level. We carefully check stable conformers whose total energy relative to that of the most stable one is less than 5 kJ/mol, because in the case of the M^+•DB18C6 complexes all the conformers that exist under the cold conditions were found to be within the range of 5 kJ/mol.[31] Vibrational analysis is carried out for the optimized structures at the same level of calculation. The oscillator strength and transition energy of electronic

transitions are obtained with TD-DFT at the M05-2X/6-31+G(d) level. For Rb and Cs, we use the Stuttgart RLC as effective core potentials (ECPs); functions of the ECPs are obtained from a database of basis sets.[37] The agreement between the calculated and observed IR spectra in the CH stretching region is not good because of Fermi resonance interactions.[31] We thus determine the structure of the complexes on the basis of their total energy and calculated electronic spectra. The binding energy of the complexes is obtained by subtracting the total energy of the complexes from the sum of the total energy of bare crown ethers and metal ions, corrected by the zero-point vibrational energy. We also calculate ΔH, ΔS and Gibbs free energy changes (ΔG) for the formation of alkali meta ion–crown ether complexes at 298.15 K and 1.0 atm on the basis of the structure of the M^+•DB18C6, M^+•B18C6 and M^+•B15C5 complexes determined experimentally and theoretically in this and our previous study.[31]

3. Results

3.1 UV and IR spectroscopy of M^+•B15C5 complexes

Figure 1 shows the UVPD spectra of the cooled M^+•B15C5 (M = Li, Na, K, Rb and Cs) complexes together with the LIF spectrum of jet-cooled B15C5 reported by Zwier and co-workers.[38,39] Except for the Li^+ complex, these UVPD spectra are measured by monitoring the yield of the M^+ photofragments. The Li^+ ion (m/z = 7) could not be detected with the second quadrupole mass filter because of its low-mass cutoff. However upon UV excitation the Li^+•B15C5 complexes produce a variety of other photofragments, and the spectrum in Fig. 1a is measured by detecting the photofragment cation at m/z = 143, which corresponds to the loss of $(OCH_2CH_2)_3$. All the M^+•B15C5 complexes show a blue shift of the absorption relative to uncomplexed B15C5. Spectroscopic studies of B15C5–$(H_2O)_n$ complexes demonstrated that the

attachment of H_2O molecules to the α oxygen atoms (O3 and O15, see Scheme 1) through the O–H•••O hydrogen bond causes a blue-shift of the S_1–S_0 absorption.[38,39] This suggests that the metal ions in the M^+•B15C5 complexes are bound to the α oxygen atoms. The Li^+ complex shows the most blue-shifted band origin, indicating the strongest interaction. The K^+•B15C5 complex shows a large red shift of the origin band (K-I) from that of the Na^+•B15C5 complex (Na-I), suggesting that a significant change in the encapsulation structure occurs between the Na^+ and K^+ complexes. For the K^+, Rb^+ and Cs^+ complexes, the band origins (K-I, Rb-I and Cs-I) gradually shift to the red with increasing ion size, implying that the interaction between the α oxygen atoms and the metal ion becomes progressively weaker from K^+ to Cs^+.

All the UVPD spectra in Figs. 1a–e show a number of vibronically resolved bands. The vibronic structure of the complexes is different in the series between Li^+, Na^+ and K^+. The UVPD spectrum of the Li^+ complex has congested features around the origin band at 36612 cm^{-1} (Li-I). In the spectrum of the Na^+ complex, the band origin is clearly observed at 36555 cm^{-1} (Na-I), accompanied by several vibronic bands. The vibronic pattern around Na-I can also be found in the higher energy region of the same spectrum (Fig. 2S); these higher energy patterns are due to vibrations of the benzene ring.[40,41] The K^+ complex shows three different vibronic patterns, which are labeled K-I, K-II and K-III in Fig. 1c. The origin band is observed at 36256 cm^{-1} (K-I), and the vibronic pattern around K-I can be seen also in the higher energy region of the same spectrum (Fig. 3S of the Supporting Information). The vibronic patterns of K-II (~36500 cm^{-1}) and K-III (~36800 cm^{-1}) consist of many sharp bands, and K-III is more congested than K-II. Similar vibronic patterns can be seen also in the UVPD spectra of the Rb^+ (Rb-I, Rb-II and Rb-III) and Cs^+ (Cs-I, Cs-II and Cs-III) complexes, which

progressively shift to the red from K^+ to Cs^+. These results suggest that there are three different conformers for each of the K^+, Rb^+ and Cs^+ complexes.

We determine the number of conformers with significant population in the ion trap and examine which peaks in the UV spectra belong to different conformers by IR-UV double resonance spectroscopy. Figure 2 shows the IR-UV spectra of the Li^+•B15C5 and Na^+•B15C5 complexes in the CH stretching region; these IR spectra are measured by monitoring the intensity of the vibronic bands labeled Li-I, Li-II and Na-I in Fig. 1 as the wavenumber of the IR OPO is scanned. For the Li^+•B15C5 complex, we find two different IR spectra, indicating that it can adopt two different conformations in the ion trap, whereas the Na^+•B15C5 complex shows only one IR spectrum and hence exists as a single conformer. The IR spectra of Li-II and Na-I show similar features (Figs. 2b and 2c), demonstrating the resemblance of the conformation for Li-II and Na-I. As described in Section 3.2 below, we use this result for the determination of the conformation.

Figure 3 displays the IR-UV spectra of the K^+•B15C5, Rb^+•B15C5 and Cs^+•B15C5 complexes in the CH stretching region. Vibronic patterns I–III in each of the UVPD spectra of the K^+•B15C5, Rb^+•B15C5 and Cs^+•B15C5 complexes show different IR features, which confirms that they arise from three different conformers. In addition, patterns I–III each show similar spectral features in the CH stretching region for the K^+, Rb^+ and Cs^+ complexes, indicating a similar conformation.

3.2 Structure of M^+•B15C5 complexes

Conformer-specific infrared spectra of the Li^+•B15C5 and Na^+•B15C5 complexes indicate that there are two and one conformers in the cold trap, respectively. We determine the structure of these conformers with the aid of quantum chemical

calculations, under the assumption that one of the two Li^+ conformers adopts a conformation similar to that of the single Na^+ conformer. Figure 4 displays the S_1–S_0 electronic spectra of the M^+•B15C5 complexes calculated with TD-DFT at the M05-2X/6-31+G(d) level. In order to compare the calculated electronic spectra with the UVPD spectra, we employ a scaling factor of 0.8340 for the transition energy calculated, which was determined to reproduce the observed transition energy of the origin band of the K^+•DB18C6 complex in our previous study.[31] Figure 5 shows the structure of the Li^+•B15C5 and Na^+•B15C5 complexes optimized at the M05-2X/6-31+G(d) level of theory. (Other stable isomers of the Li^+•B15C5 and Na^+•B15C5 complexes are displayed in Figs. 10S and 11S, respectively.) In the case of the Na^+•B15C5 complex, one conformer (Na-A in Fig. 5c) is significantly more stable than the others; the energy difference between the most stable (Na-A) and the second most stable (Na-B in Fig. 11S) conformers is 4.56 kJ/mol. In addition, the energy of the S_1–S_0 transition calculated for Na-A agrees well with the position of the origin band (Na-I) of the Na^+ complex (Fig. 4b). Therefore, we assign the single conformer of the Na^+•B15C5 complex to Na-A. The B15C5 part in Na-A adopts an open form, in which the dihedral angle of C14–O15–C1–C16 and C4–O3–C2–C19 (see Scheme 1) is not so large, and the Na^+ ion is positioned at the center of the ether ring.

For the Li^+•B15C5 complex, five conformers have the total energy lower than 5 kJ/mol relative to that of the most stable one at the M05-2X/6-31+G(d) level (Fig. 10S). We also calculate the total energy of these conformers at a higher level [wB97XD/6-31++G(d,p)] and find that three of the five forms (Li-A, Li-B and Li-C in Fig. 10S) are substantially more stable than the others; the total energy of the third most stable conformer relative to that of the most stable one is ~0.36 kJ/mol, whereas the energy difference between the third and fourth ones is 3.38 kJ/mol. Therefore, it is

reasonable to assign the two conformers showing Li-I and Li-II in the UVPD spectrum to two of the three stable isomers. Since the IR spectrum of Li-II resembles that of Na-I (Fig. 2), the conformation of Li-II should be similar to that of Na-I. Li-C has a conformation similar to that of Na-A among the three stable isomers of the Li^+ complex (Fig. 5). Therefore, Li-II is attributed to Li-C. In addition, since the band position of Li-A is more close to Li-I than Li-B (see Fig. 16S), we assign the conformer of Li-I to Li-A (Fig. 5).

For the K^+, Rb^+ and Cs^+ complexes, there are 6, 5, and 4 conformers calculated to be within 5 kJ/mol, respectively (Figs. 12S–14S). In these conformers we can find four groups based on the similarity of the conformation (two of the six conformers of the K^+ complex and one of the five forms of the Rb^+ complex are not classified into either of the four groups because of their conformations different from those of the four groups). As shown in Fig. 3, each of conformers I–III has similar IR spectra for the K^+, Rb^+ and Cs^+ complexes. Under the assumption that conformers having similar IR spectra will adopt a similar conformation, we can assign the three conformers of the K^+•B15C5, Rb^+•B15C5 and Cs^+•B15C5 complexes to three of the four conformation groups. In Figs. 4c–e, the UVPD spectra of the K^+, Rb^+ and Cs^+ complexes are compared with electronic spectra calculated for the stable isomers. Two of the four conformer groups (red and black bars in Figs. 4c–e) show good agreement with vibronic patterns I and II of the UVPD spectra. Therefore, vibronic patterns I and II of the K^+, Rb^+ and Cs^+ complexes can be assigned to these two groups, which are called conformer groups I and II hereafter. The structure of conformer groups I (K-C, Rb-D and Cs-D) and II (K-B, Rb-A and Cs-B) is displayed in Figs. 6 and 7, respectively. In the case of group I (Fig. 6), the B15C5 component adopts a C_s conformation similar to Li-C and Na-A. The ether ring opens the most by taking

planar forms for the C14–O15–C1–C16 and C4–O3–C2–C19 parts, but the difference in the structure from Li-C and Na-A is seen at the C8–O9–C10 part, as highlighted with arrows in Figs. 5 and 6. Since the cavity size of B15C5 is smaller than the ion size of K^+, Rb^+ and Cs^+, the metal ions cannot enter the ether ring in the same way as Li-C and Na-A, and they are thus positioned on the ring. Conformer group II (Fig. 7) shows slightly distorted forms; one of the dihedral angles of C14–O15–C1–C16 and C4–O3–C2–C19 is about –75°, and the other one is close to zero. Similar to group I, the metal ions in group II are located on the ether ring. For vibronic patterns III in the UVPD spectra, it is difficult to assign definitely the conformation to either of the other two groups by the electronic transition calculated with TD-DFT, because these two groups show electronic spectra similar to each other. Close inspection of the structure of these two groups (Figs. 8 and 15S) indicates that the difference in the conformation between these groups is very small, only at the O6 atom. As a result, the electronic transition is similar for these groups. We further performed quantum chemical calculations for these conformers at a higher level [wB97XD/6-31++G(d,p)]. These calculations still do not show any predominance in the stability for one group over the other, but Rb-B and Cs-A each (Fig. 8) are predicted to be more stable than Rb-C and Cs-C (Fig. 15S), respectively, with the difference in the total energy of more than 3.5 kJ/mol. In addition, the stability of K-E (Fig. 8) is almost the same as that of K-A (Fig. 15S) by less than 1 kJ/mol. Therefore, it is more reasonable to assign the third conformer of the K^+, Rb^+ and Cs^+ complexes to K-E, Rb-B and Cs-A (Fig. 8). The structure of the K^+•B15C5 complexes in Figs. 6–8 is in agreement with the form proposed for the K^+•15C5 complex by Martínez-Haya and co-workers.[24,26]

The relation between the vibronic structure and the conformation for the M^+•B15C5 complexes is consistent with that found for bare B15C5. Zwier and

co-workers suggested in their papers on UV and IR spectroscopy of jet-cooled B15C5 and 4'-amino-benzo-15-crown-5 (ABC) that the vibronic structure around the band origin is a good diagnosis of the conformation around the phenyl ring.[38,39] For B15C5 and ABC, conformers in which the β carbon atoms (C4 and C14) are displaced largely from the plane of the phenyl ring show extensive and intense Franck-Condon progressions.[38,39] This relation can be seen also in the UVPD spectra of the K^+•B15C5, Rb^+•B15C5 and Cs^+•B15C5 complexes. In conformers I of the K^+, Rb^+ and Cs^+ complexes (Fig. 6), both of the dihedral angles of C14–O15–C1–C16 and C4–O3–C2–C19 are close to zero. These conformers show strong origin bands (K-I, Rb-I and Cs-I in Fig. 1) and weak progressions. In conformers II and III (Figs. 7 and 8), one of the dihedral angles is largely displaced from zero. It follows that the UV spectra of these conformers show extensive and intense progressions. In addition, the dihedral angle of conformer III (Fig. 8) is larger than that of conformer II (Fig. 7), providing more congested progressions for conformer III than for conformer II.

3.3 UV and IR spectroscopy of M^+•B18C6 complexes

Figure 9 shows the UVPD spectra of the cooled M^+•B18C6 (M = Li, Na, K, Rb and Cs) complexes, together with the LIF spectrum of jet-cooled B18C6 reported by Ebata and co-workers.[42,43] These UVPD spectra are measured by monitoring the yield of the M^+ photofragment ions except for the Li^+•B18C6 complex; the spectrum of the Li^+ complex in Fig. 9a is measured by detecting the photofragment cation at m/z = 231, which corresponds to the loss of $(OCH_2CH_2)_2$. All the M^+•B18C6 complexes show a blue shift of the absorption relative to uncomplexed B18C6, indicating that the metal ions are attached to O3 and O18 oxygen atoms (see Scheme1). The Li^+ complex shows an origin band at 36694 cm^{-1} (Li-i), but there is another strong band (Li-ii) at a

position (36698 cm^{-1}) very close to Li-i. In the UV spectrum of the Na^+ complex, we find three different vibronic patterns, which are labeled Na-i, Na-ii and Na-iii. For the K^+•B18C6 complex, two different patterns (K-i and K-ii) are found from 36101 and 36398 cm^{-1}. The Rb^+•B18C6 and Cs^+•B18C6 complexes each show only one vibronic pattern (Rb-i and Cs-i). The vibronic patterns around K-i, K-ii, Rb-i and Cs-i are repeatedly seen in the higher wavenumber region (Figs. 7S–9S).

Figure 10 shows conformer-specific IR spectra of the M^+•B18C6 complexes in the CH stretching region measured using the vibronic bands labeled in Fig. 9 *via* IR-UV double resonance. On this basis we determine the number of conformers as 2, 3, 2, 1 and 1 for the Li^+, Na^+, K^+, Rb^+ and Cs^+ complexes in the cold ion trap, respectively. The IR spectra of K-ii, Rb-i and Cs-i (Figs. 10g–i) are similar to each other, suggesting that the conformation is similar for K-ii, Rb-i and Cs-i. This seems reasonable also from the position of the origin bands in the UVPD spectra (Fig. 9) that K-ii, Rb-i and Cs-i progressively and regularly shift to the red with increasing metal size.

3.4 Structure of M^+•B18C6 complexes

In Fig. 11 we show calculated electronic band origins for stable conformers of the M^+•B18C6 complexes and compare them with the UVPD spectra. Figures 12–14 display the structure of the M^+•B18C6 complexes optimized at the M05-2X/6-31+G(d) level with the Stuttgart RLC potential for Rb and Cs. In the case of the Li^+•B18C6 complex, there are only two conformers (Li-a and Li-b in Fig. 12) within a total energy of less than 5 kJ/mol. Li-a and Li-b show the electronic transition energies close to the band origins Li-i and Li-ii (Fig. 11a). We can determine which conformer of Li-a or Li-b corresponds to Li-i or Li-ii by comparing results of vibrational analysis of Li-a and

Li-b at the M05-2X/6-31+G(d) level with low-frequency progressions of Li-i and Li-ii emerging in the UVPD spectrum. The vibrational analysis of Li-a predicts 21, 37 and 58 cm^{-1} for the three lowest-frequency vibrations, while Li-b has vibrations of 24, 66 and 67 cm^{-1}. We distinguish peaks in the UVPD spectrum of the Li^+ complex that belong to Li-i and Li-ii *via* IR-UV double resonance, as displayed in Fig. 6S. Li-i is accompanied by low-frequency bands of 55 and 64 cm^{-1}. Li-ii shows two lower frequency vibrations (30 and 35 cm^{-1}), which are in agreement with the two lowest-frequency vibrations of Li-a. We therefore attribute Li-i and Li-ii to Li-b and Li-a in Fig. 12, respectively. Geometry optimization of the Na^+•B18C6 complex at the M05-2X/6-31+G(d) level predicts six conformers within 5 kJ/mol of the total energy (Fig. 18S). As seen in Fig. 11, since the most and the third most stable conformers (Na-a and Na-c) well reproduce the band positions of Na-iii and Na-ii, we assign Na-ii and Na-iii to Na-c and Na-a, respectively. The second most stable conformer (Na-b) has a conformation very similar to that of Na-a, and their respective S_1–S_0 transition energies are similarly close (Fig. 22S). However, the vibronic structure built on the band origin of Na-iii is reproduced with regular progressions, and there is no evidence for the coexistence of two conformers in this region. Therefore, Na-iii is tentatively attributed to the most stable form (Na-a). The similarity of the conformation for Na-a and Na-b suggests that the potential barrier between Na-a and Na-b may not be so high, such that Na-b may transfer to Na-a in the cooling process. For Na-i, we can attribute the structure to the fourth most stable form (Na-d). The vibronic structure of Na-i shows extensive low-frequency progressions, implying a large structural change upon the S_1–S_0 excitation. Consequently, the conformations of Na-i, Na-ii and Na-iii are ascribed to Na-d, Na-c and Na-a (Fig. 13), respectively.

The determination of the structure of the K^+•B18C6, Rb^+•B18C6 and Cs^+•B18C6 complexes can be done in parallel under the assumption that K-ii, Rb-i and Cs-i have a similar conformation. Figure 14 displays stable conformers of K^+•B18C6, Rb^+•B18C6 and Cs^+•B18C6 optimized at the M05-2X/6-31+G(d) level and the Stuttgart RLC potential for Rb and Cs. Geometry optimization of the K^+•B18C6, Rb^+•B18C6 and Cs^+•B18C6 complexes predicts 5, 3 and 5 stable conformers within 5 kJ/mol (Figs. 19S–21S). Among these conformers, the most stable ones (K-a, Rb-a and Cs-a) have a similar conformation (Fig. 14). As seen in Fig. 11, the S_1–S_0 transition energy predicted for K-a, Rb-a and Cs-a is in good agreement with the positions of K-ii, Rb-i and Cs-i, respectively. We therefore attribute the conformer of K-ii, Rb-i and Cs-i to K-a, Rb-a and Cs-a, respectively. For K-i, since the second most stable conformer (K-b) well replicates the position of K-i, the conformation of K-i is ascribed to K-b. The structure of the M^+•B18C6 complexes mentioned above are similar to those proposed for the M^+•18C6 complexes in previous reports.[18–20,22,23,25,27–29,31]

4. Discussion

4.1 Effect of phenyl group substitution and ether ring size to the encapsulation of crown ethers

Since we unambiguously determine the structures of the M^+•B15C5, M^+•B18C6 and M^+•DB18C6 complexes in this and our previous study,[31] we can discuss the effect of phenyl group substitution and ether ring size to the encapsulation of alkali metal ions on the basis of these conformers. As seen in a stable D_{3d} conformer of K^+•18C6 (Fig. 23S), the O–C–C–O linkages in crown ethers prefer to assume gauche conformations. Phenyl attachment to part of ether ring decreases the ring flexibility because of structural constraints due to the delocalization (aromatic) energy. In

benzo-crown ethers, α oxygen atoms (O3 and O18 in B18C6) are located in the same plane of the phenyl ring; this is an unavoidable requirement for benzo-crown ethers. In all the conformers of the M^+•B18C6 complexes (Figs. 12–14), O18–C1–C2–O3 atoms are located in the same plane (eclipsed conformations), whereas the other O–C–C–O parts take gauche conformations. In the M^+•DB18C6 complexes, two O–C–C–O parts adjacent to the benzene rings adopt eclipsed conformations.[31] Furthermore, benzo-crown ethers are likely to take planar forms at the β carbon atoms (C4 and C17 in B18C6) for gaining the delocalization energy by extending π MOs to the α oxygen atoms; in the case of 1,2-dimethoxybenzene monomer, the carbon and oxygen atoms of the methoxy groups are positioned in the same plane of the benzene ring.[44] However, this condition is not so strict, and the conformation at the β carbon atoms depends on the metal ion encapsulated. In the stable conformers of the Li^+•B18C6 and Na^+•B18C6 complexes (Figs. 12 and 13), the dihedral angle of the C17–O18–C1–C19 and/or C4–O3–C2–C22 part is displaced largely from zero. In this case, the M^+–O interaction is too strong to keep planar forms at the β carbon atoms. For K^+, Rb^+ and Cs^+ ions, the M^+–O interaction is weaker, and as a result, the β carbon atoms in the K^+•B18C6, Rb^+•B18C6 and Cs^+•B18C6 complexes (Fig. 14) are located in the plane of the phenyl ring to gain the delocalization energy. Similar to the case of the M^+•B18C6 complexes, the M^+•DB18C6 ions adopt distorted forms for M = Li and Na (Fig. 5 in Ref. 31) and planar ones for M = K, Rb and Cs (Fig. 6 in Ref. 31) at the β carbon atoms.

The effect of phenyl group substitution can be found in the results of the binding energy and the number of stable conformers for M^+•DB18C6 and M^+•B18C6. Figure 24S of the Supporting Information shows the binding energy of the M^+•DB18C6,

M^+•B18C6 and M^+•B15C5 complexes calculated for the stable conformers. The binding energy of the M^+•B18C6 complexes is higher than that of M^+•DB18C6 for each of alkali metal ions. Thanks to a more flexible nature for B18C6 than for DB18C6, the M^+•B18C6 complexes can adopt conformations more efficient for ion encapsulation than M^+•DB18C6, giving larger binding energies. In addition, reduced flexibility for DB18C6 decreases the number of conformers. Table 1 shows the number of conformers found for the M^+•B15C5, M^+•B18C6 and M^+•DB18C6 complexes under the cold conditions of our ion trap together with that of jet-cooled monomers.[31,38,42,43] DB18C6 monomer has smaller number of conformers (2) than B18C6 monomer (4). This trend is seen also for the metal ion complexes; the number of conformations for the M^+•DB18C6 complexes is equal to or less than those of M^+•B18C6 for all the alkali metal ions.

For crown ethers with smaller rings, the number of possible conformations is thought to be smaller than that with larger ones, because the combination of gauche and eclipse conformations in the ether ring may be limited for smaller ethers. B18C6 monomer has in fact more conformers (4) than B15C5 (3). Nevertheless, a similar trend in the conformation number is not necessarily observed for the M^+•B15C5 and M^+•B18C6 complexes. The number of conformations of M^+•B15C5 complexes is equal to or less than that of M^+•B18C6 for M = Li and Na, but M^+•B15C5 adopts more conformations than M^+•B18C6 for M = K, Rb and Cs. This result suggests that the poor flexibility of B15C5 prevents the ether ring from taking one exceptionally stable conformation with K^+, Rb^+ and Cs^+. Therefore, we cannot state a general relation between the ether ring size and the number of conformers from the results of M^+•B15C5 and M^+•B18C6.

In order to demonstrate the difference in the ion-complex structure among B15C5, B18C6 and DB18C6 more quantitatively, we derive structural parameters from the conformers of the M^+•B15C5, M^+•B18C6 and M^+•DB18C6 complexes (Fig. 15). The definition of the structural parameters is described in Fig. 15a: R is the distance between the oxygen atoms and the metal ion, and h_O and h_M are the distance of the oxygen atoms and the metal ion, respectively, from the mean plane of all the oxygen atoms. A similar analysis was performed by Dearden and co-workers.[17] Circles in Figs. 15b–d represent the values of each conformer; vertical bars in Figs. 15b and 15c denote the standard deviation of R and h_O calculated for all the oxygen atoms in each conformer. As seen in Fig. 15b, R increases monotonously from Li^+ to Cs^+. In addition, no significant difference in R can be seen among B15C5, B18C6 and DB18C6 for each metal ion, indicating that the distance R does not depend either on the ether ring size or on the number of phenyl groups. The distribution of R values is quite narrow for all the conformers; the metal ions in these conformers are equally bonded to all the oxygen atoms. This result is in contrast to the prediction of quantum chemical calculations in a previous study that Li^+ ion is bonded mainly to three of six oxygen atoms in the Li^+•18C6 complex.[23] The difference among B15C5, B18C6 and DB18C6 can be clearly seen in Figs. 15c and 15d. In the case of h_O (Fig. 15c), all the conformers of the M^+•B18C6 and M^+•DB18C6 complexes with M = Li and Na and one of the Li^+•B15C5 conformers (Li-A in Fig. 5) have substantially larger values (~0.8 Å) with wider distributions. In these conformers the oxygen atoms are arranged in a three-dimensional manner, similar to the octahedral-type coordination in Li-a (Fig. 12a). For larger conformers the distance h_O becomes smaller and its distribution narrower, showing that the oxygen atoms in these conformers are positioned close to the mean plane and form two-dimensional circles.

Figure 15d represents the distance of the metal ion from the mean plane of the oxygen atoms in each conformer. The distance h_M in the K^+•18C6 complex with D_{3d} symmetry (Fig. 23S) is zero. For the Li^+ and Na^+ complexes of M^+•B15C5, h_M is close to zero, indicating that the Li^+ and Na^+ ions in the M^+•B15C5 conformers can be positioned at the center of a three-dimensional ring (Li-A in Fig. 5) or a two-dimensional circle (Li-C and Na-A in Fig. 5). For K^+, Rb^+ and Cs^+ ions, the ion size is too large to enter the cavity of B15C5, and these metal ions are largely apart from the mean plane of the oxygen atoms with distances of ~1.46, ~1.80, and ~2.01 Å, respectively. In the case of the M^+•B18C6 and M^+•DB18C6 complexes, h_M is close to zero for Li^+ and Na^+; these metal ions are held at the center of a three-dimensional ring (Figs. 12 and 13). In the K^+•B18C6 and K^+•DB18C6 complexes, h_M is still small (~0.4 Å), but is not completely zero like the K^+•18C6 complex with D_{3d} symmetry; the phenyl groups in B18C6 and DB18C6 reduce the flexibility of the ether rings, and the K^+ ion falls slightly from the center of the rings. The distance h_M goes up to ~1.0 and ~1.3 Å for the Rb^+ and Cs^+ complexes of B18C6 and DB18C6, showing that Rb^+ and Cs^+ ions cannot enter the cavity of B18C6 and DB18C6. However, h_M of the B18C6 and DB18C6 complexes with Rb^+ and Cs^+ is substantially smaller than that of the B15C5 complexes (~1.80 and ~2.01 Å, respectively).

4.2 Relation between complex structure and ion selectivity of crown ethers

As previously reviewed by Izatt and co-workers, 18C6, B18C6 and DB18C6 have higher equilibrium constant for binding K^+ compared to the other alkali metal ions in solution.[3] (The measured equilibrium constants in Ref. 3 are collected in Fig. 25S.) The calculated binding energies of the M^+•B18C6 and M^+•DB18C6 complexes (Fig. 24S) decrease monotonically with increasing the metal size. Since larger binding energy leads to larger equilibrium constant, the trend in the binding energy of B18C6

and DB18C6 with K^+, Rb^+ and Cs^+ is in agreement with the decrease in the equilibrium constant from K^+ to Cs^+. However, the decrease in the binding energy from Li^+ to K^+ is inconsistent with this trend. Therefore, the solvent effect will govern the encapsulation ability in solution, especially for smaller ions. In order to examine the solvent effect to the complex formation, we calculate and compare thermochemical values under isolated and hydrated conditions. Figure 16 displays ΔH, ΔS and ΔG for the complex formation between $M^+\bullet(H_2O)_n$ and DB18C6 with M = Li, Na, K, Rb and Cs and n = 0 and 1 at 298.15 K and 1.0 atm. (Thermochemistry data for B18C6 and B15C6 are shown in Figs. 26S and 27S.) These values are calculated on the basis of the most stable conformers of the $M^+\bullet$DB18C6 complexes.[31] For the n = 1 complexes we perform geometry optimization and vibrational analysis by attaching one H_2O molecule to the most stable conformers of $M^+\bullet$DB18C6 complexes before calculating these thermochemistry data. (Optimized structures of the $M^+\bullet$DB18C6$\bullet H_2O$ and $M^+\bullet H_2O$ complexes are shown in Figs. 28S and 31S.) ΔH of the n = 0 complexes increases from Li^+ to Cs^+. In contrast, ΔS shows similar values (~ –170 $J\bullet mol^{-1}\bullet K^{-1}$) for all the metal ions. ΔG of the n = 0 complexes increases from Li^+ to Cs^+ because of the increase of ΔH. Attachment of one H_2O molecule changes ΔH largely from that of n = 0. The ΔH values of n = 1 are substantially larger than those of n = 0 for Li^+ and Na^+, whereas the difference in ΔH between n = 0 and 1 is small for Rb^+ and Cs^+. ΔS with one H_2O molecule is still insensitive to the metal ions, similar to that of n = 0. As a result, the difference in ΔG between the metal ions becomes smaller for n = 1 than that for n = 0. The tendency in the change in ΔH from n = 0 to 1 can be understood from the structure of the stable conformers. (The relation between ΔH for the complex formation and the stabilization energy by solvation is displayed in Fig. 32S.) In the $M^+\bullet$B18C6 and $M^+\bullet$DB18C6 complexes, Li^+ and Na^+ are fully surrounded by the ether

ring, as shown in Figs. 12 and 13, and Fig. 5 in Ref. 31. The stabilization energy of M^+•B18C6 and M^+•DB18C6 (M = Li and Na) by solvation will be much smaller than that of bare metal ions, providing large difference in ΔH between $n = 0$ and 1. In the Rb^+ and Cs^+ complexes of B18C6 and DB18C6, the metal ions are located largely apart from the ether ring (Fig. 14 and Fig. 6 in Ref. 31) and can be solvated by solvent molecules along with the crown ethers. The stabilization energy of the complexes by solvation will be comparable to that of bare metal ions, showing small difference in ΔH between $n = 0$ and 1.

Thermochemistry and kinetic data for the complex formation in solution have been reported for many kinds of crown ethers, metal ions and solvents.[3,45] Comparison of thermochemistry data calculated on the basis of the stable complexes (Fig. 16) with those measured in solution reveals the main factor dominating the ion selectivity in solution. In the case of the DB18C6 complexes with alkali metal ions in solution, ΔH and ΔS were reported only for Na^+ and K^+, although there are a number of studies of the equilibrium constants. Most of the ΔS values for the formation of the Na^+•DB18C6 and K^+•DB18C6 complexes in solution are in the range from –20 to –120 $J•mol^{-1}•K^{-1}$, which are more or less similar to the calculated ΔS in Fig. 16.[3,45] In contrast, the ΔH values in solution are –20 ~ –50 $kJ•mol^{-1}$, which are almost one order of magnitude smaller than those in Fig. 16. Wang et al. reported thermochemical values for the formation of K^+•18C6 in water at the temperature of 298.15–398.15 K; ΔH and ΔS are about –25 $kJ•mol^{-1}$ and –50 $J•mol^{-1}•K^{-1}$,[46] similar to the values of the DB18C6 complexes in solution mentioned above.[3,45] The ΔG values in Fig. 16 do not show any preference for K^+, but the difference in ΔG among alkali metal ions becomes smaller from $n = 0$ to 1. ΔH will increase more for smaller ions (Li^+ and Na^+) than for K^+ by

the solvation, as predicted from the results in Fig. 16. This will change the order of ΔG from that in the gas phase and show substantial selectivity for K^+ in solution. Therefore, we can propose that the ion selectivity of crown ethers in solution is mainly driven by ΔH, which is strongly affected by the complex structure. A similar conclusion was drawn by Wang et al. and Inoue et al. in their thermodynamic studies of complex formation in solution.[46–48]

On the other hand, the results of B15C5 exhibit another aspect of the ion selectivity. In the case of B15C5, the structure of the Na^+•B15C5 complex (Fig. 5c) demonstrates the optimum matching in size between B15C5 and Na^+ ion. Nevertheless, a clear preference for Na^+ is not necessarily seen for 15C5 and B15C5 in the results of the equilibrium constant (Fig. 25S); in some kinds of solution the constant for Na^+ is almost the same or smaller than that for K^+, Rb^+ and Cs^+. This can be explained partly with the encapsulation manner characteristic of B15C5. The K^+•B15C5, Rb^+•B15C5 and Cs^+•B15C5 complexes each have three conformers as shown in Figs. 6–8, while the Na^+•B15C5 complex adopts only one conformation. A larger number of conformations is entropically advantageous for the formation of the complex, which will increase equilibrium constants for K^+, Rb^+ and Cs^+.

Rodriguez and Lisy recently reported the hydration structure in gas-phase M^+•18C6•$(H_2O)_{1–4}$ complexes investigated by IR spectroscopy.[27] The structures they proposed for hydrated Rb^+•18C6 and Cs^+•18C6 complexes are consistent with what one might expect from the structures of the bare M^+•B18C6 and M^+•DB18C6 complexes determined in this study; H_2O molecules are bound on the open side of the complexes. In contrast, they propose that addition of one H_2O molecule to the Li^+•18C6 and Na^+•18C6 complexes opens the ether rings, which if correct would represent a

significant change in structure of the bare complexes of M^+•B18C6 and M^+•DB18C6 with M = Li and Na. In addition, there is still an ambiguity for the number and the structure of the M^+•18C6•$(H_2O)_{1-4}$ complexes, which seem difficult to be determined by IR spectroscopy alone. In this and our previous paper, we determine the number and the structure of the conformers for bare M^+•B15C5, M^+•B18C6 and M^+•DB18C6 complexes by UV and IR spectroscopy.[31] Application of our double resonance approach to hydrated crown ether complexes should allow to further clarify picture of selective capture of crown ethers in solution.

5. Summary

We have measured UV photodissociation (UVPD) and IR-UV double resonance spectra of the M^+•B15C5 and M^+•B18C6 (M = Li, Na, K, Rb and Cs) complexes produced by nanoelectrospray and cooled to ~10 K in a 22-pole ion trap. We have determined the number and the structure of the conformers of M^+•B15C5 and M^+•B18C6 with the aid of quantum chemical calculations. The number of conformers for the M^+•DB18C6 complexes is equal to or smaller than those of M^+•B18C6, which seems to come from increased rigidity of the ether ring for DB18C6. In contrast, the B15C5 complexes with K^+, Rb^+ and Cs^+ have a larger number of conformers than B18C6. In these cases, the fact that the metal ion does not fit easily into the ether ring allows more conformational flexibility. In the Na^+•B15C5 and K^+•B18C6 complexes, the ether rings hold the metal ions in their center, demonstrating an optimal matching in size between the cavity of the crown ethers and the metal ions. However, the binding energy for the M^+•B15C5, M^+•B18C6, and M^+•DB18C6 complexes show monotonic change, giving no direct signature of the selective capture of crown ethers. By calculating thermochemistry values on the basis of the stable conformers and comparing them with those observed in solution we conclude that the ion selectivity of crown

ethers in solution is mainly driven by the enthalpy change, which strongly depends on the complex structure. Extending our techniques to partially solvated crown ether complexes should further elucidate the picture of selective capture of crown ethers in solution.

Acknowledgment

This work is supported by Grant-in-Aids (Grant No. 21350016) for Scientific Research from the Ministry of Education, Culture, Sports, Science, and Technology (MEXT) of Japan, the Swiss National Science foundation through grant 200020_130579 and École Polytechnique Fédérale de Lausanne (EPFL). YI also thanks the support from the Excellent Young Researchers Overseas Visit Program of Japan Society for the Promotion of Science (JSPS).

Supporting Information Available: Results of IR-UV double resonance spectroscopy, analysis of the vibronic structure in the UVPD spectra, optimized structures, calculated electronic spectra, binding energies and thermochemistry data calculated on the basis of the stable conformers, and a full list of authors of Ref. 36. This material is available free of charge *via* the internet at http://pubs.acs.org.

References

[1] Pedersen, C. J. *J. Am. Chem. Soc.* **1967**, *89*, 7017–7036.

[2] Pedersen, C. J. *Science* **1988**, *241*, 536–540.

[3] Izatt, R. M.; Bradshaw, J. S.; Nielsen, S. A.; Lamb, J. D.; Christensen, J. J. *Chem. Rev.* **1985**, *85*, 271–339, and references therein.

[4] Allen F. H. *Acta Cryst.* **2002**, *B58*, 380–388.

[5] Zhang, H.; Chu, I.-H.; Leming, S.; Dearden, D. V. *J. Am. Chem. Soc.* **1991**, *113*, 7415–7417.

[6] Zhang, H.; Dearden, D. V. *J. Am. Chem. Soc.* **1992**, *114*, 2754–2755.

[7] Maleknia, S.; Brodbelt, J. *J. Am. Chem. Soc.* **1992**, *114*, 4295–4298.

[8] Chu, I.-H.; Zhang, H.; Dearden, D. V. *J. Am. Chem. Soc.* **1993**, *115*, 5736–5744.

[9] Brodbelt, J. S.; Liou, C.-C. *Pure & Appl. Chem.* **1993**, *65*, 409–414.

[10] Dearden, D. V.; Zhang, H.; Chu, I.-H.; Wong, P.; Chen, Q. *Pure & Appl. Chem.* **1993**, *65*, 423–428.

[11] Ray, D.; Feller, D.; More, M. B.; Glendening, E. D.; Armentrout, P. B. *J. Phys. Chem.* **1996**, *100*, 16116–16125.

[12] Sobott, F.; Kleinekofort, W.; Brutschy, B. *Anal. Chem.* **1997**, *69*, 3587–3594.

[13] More, M. B.; Ray, D.; Armentrout, P. B. *J. Phys. Chem. A* **1997**, *101*, 4254–4262.

[14] More, M. B.; Ray, D.; Armentrout, P. B. *J. Phys. Chem. A* **1997**, *101*, 7007–7017.

[15] More, M. B.; Ray, D.; Armentrout, P. B. *J. Am. Chem. Soc.* **1999**, *121*, 417–423.

[16] Armentrout, P. B. *Int. J. Mass Spectrom.* **1999**, *193*, 227–240.

[17] Anderson, J. D.; Paulsen, E. S.; Dearden, D. V. *Int. J. Mass Spectrom.* **2003**, *227*, 63–76.

[18] Lee, S.; Wyttenbach, T.; von Helden, G.; Bowers, M. T. *J. Am. Chem. Soc.* **1995**, *117*, 10159–10160.

[19] Wyttenbach, T.; von Helden, G.; Bowers, M. T. *Int. J. Mass Spectrom. Ion Proc.* **1997**, *165/166*, 377–390.

[20] Rodriguez, J. D.; Vaden, T. D.; Lisy, J. M. *J. Am. Chem. Soc.* **2009**, *131*, 17277–17285.

[21] Rodriguez, J. D.; Lisy, J. M. *J. Phys. Chem. A* **2009**, *113*, 6462–6467.

[22] Rodriguez, J. D.; Lisy, J. M. *Int. J. Mass Spectrom.* **2009**, *283*, 135–139.

[23] Rodriguez, J. D.; Kim, D.; Tarakeshwar, P.; Lisy, J. M. *J. Phys. Chem. A* **2010**, *114*, 1514–1520.

[24] Martínez-Haya, B.; Hurtado, P.; Hortal, A. R.; Steill, J. D.; Oomens, J.; Merkling, P. J. *J. Phys. Chem. A* **2009**, *113*, 7748–7752.

[25] Martínez-Haya, B.; Hurtado, P.; Hortal, A. R.; Hamad, S.; Steill, J. D.; Oomens, J. *J. Phys. Chem. A* **2010**, *114*, 7048–7054.

[26] Hurtado, P.; Hortal, A. R.; Gámez, F.; Hamad, S.; Martínez-Haya, B. *Phys. Chem. Chem. Phys.* **2010**, *12*, 13752–13758.

[27] Rodriguez, J. D.; Lisy, J. M. *J. Am. Chem. Soc.* **2011**, *133*, 11136–11146.

[28] Kim, H. J.; Shin, W. J.; Choi, C. M.; Lee, J. H.; Kim, N. J. *Bull. Korean Chem. Soc.* **2008**, *29*, 1973–1976.

[29] Choi, C. M.; Kim, H. J.; Lee, J. H.; Shin, W. J.; Yoon, T. O.; Kim, N. J.; Heo, J. *J. Phys. Chem. A* **2009**, *113*, 8343–8350.

[30] Choi, C. M.; Lee, J. H.; Choi, Y. H.; Kim, H. J.; Kim, N. J.; Heo, J. *J. Phys. Chem. A* **2010**, *114*, 11167–11174.

[31] Inokuchi, Y.; Boyarkin, O. V.; Kusaka, R.; Haino, T.; Ebata, T.; Rizzo, T. R. *J. Am. Chem. Soc.* **2011**, *133*, 12256–12263.

[32] Boyarkin, O. V.; Mercier, S. R.; Kamariotis, A.; Rizzo, T. R. *J. Am. Chem. Soc.* **2006**, *128*, 2816–2817.

[33] Rizzo, T. R.; Stearns, J. A.; Boyarkin, O. V. *Int. Rev. Phys. Chem.* **2009**, *28*, 481–515.

[34] Svendsen, A.; Lorenz, U. J.; Boyarkin, O. V.; Rizzo, T. R. *Rev. Sci. Instrum.* **2010**, *81*, 073107 (7 pages).

[35] Mohamadi, F.; Richards, N. G. J.; Guida, W. C.; Liskamp, R.; Lipton, M.; Caufield, C.; Chang, G.; Hendrickson, T.; Still, W. C. *J. Comput. Chem.* **1990**, *11*, 440–467.

[36] Gaussian 09, Revision A.02, Frisch M. J. et al., Gaussian, Inc., Wallingford CT, 2009.

[37] Schuchardt, K. L.; Didier, B. T.; Elsethagen, T.; Sun, L.; Gurumoorthi, V.; Chase, J.; Li, J.; Windus, T. L. *J. Chem. Inf. Model.* **2007**, *47*, 1045–1052.

[38] Shubert, V. A.; James III, W. H.; Zwier, T. S. *J. Phys. Chem. A* **2009**, *113*, 8055–8066.

[39] Shubert, V. A.; Müller, C. W.; Zwier, T. S. *J. Phys. Chem. A* **2009**, *113*, 8067–8079.

[40] Okuyama, K.; Mikami, N.; Ito, M. *J. Phys. Chem.* **1985**, *89*, 5617–5625.

[41] Suzuki, T.; Ito, M. *J. Chem. Phys.* **1989**, *91*, 4564–4570.

[42] Kusaka, R.; Inokuchi, Y.; Ebata, T. *Phys. Chem. Chem. Phys.* **2007**, *9*, 4452–4459.

[43] Kusaka, R.; Inokuchi, Y.; Xantheas, S. S.; Ebata, T. *Sensors* **2010**, *10*, 3519–3548.

[44] Yi, J. T.; Ribblett, J. W.; Pratt, D. W. *J. Phys. Chem. A* **2005**, *109*, 9456–9464.

[45] Izatt, R. M.; Pawlak, K.; Bradshaw, J. S. *Chem. Rev.* **1995**, *95*, 2529–2586.

[46] Wang, P. W.; Izatt, R. M.; Gillespie, S. E.; Oscarson, J. L.; Zhang, X. X.; Wang, C.; Lamb, J. D. *J. Chem. Soc. Faraday Trans.* **1995**, *91*, 4207–4213.

[47] Inoue, Y.; Liu, Y.; Tong, L.-H.; Ouchi, M.; Hakushi, T. *J. Chem. Soc. Perkin Trans. 2* **1993**, 1947–1950.

[48] Inoue, Y.; Hakushi, T.; Liu, Y.; Tong, L.-H. *J. Org. Chem.* **1993**, *58*, 5411–5413.

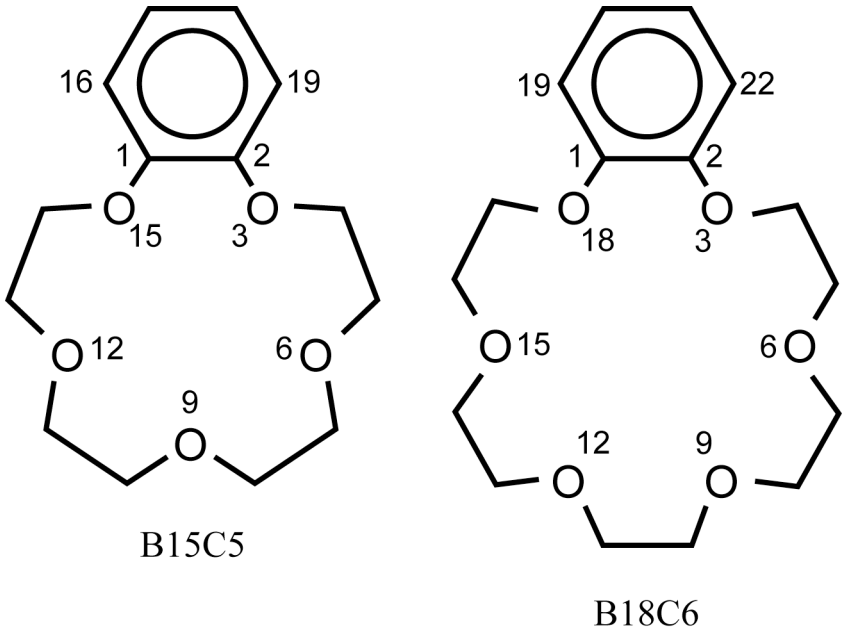

Scheme 1

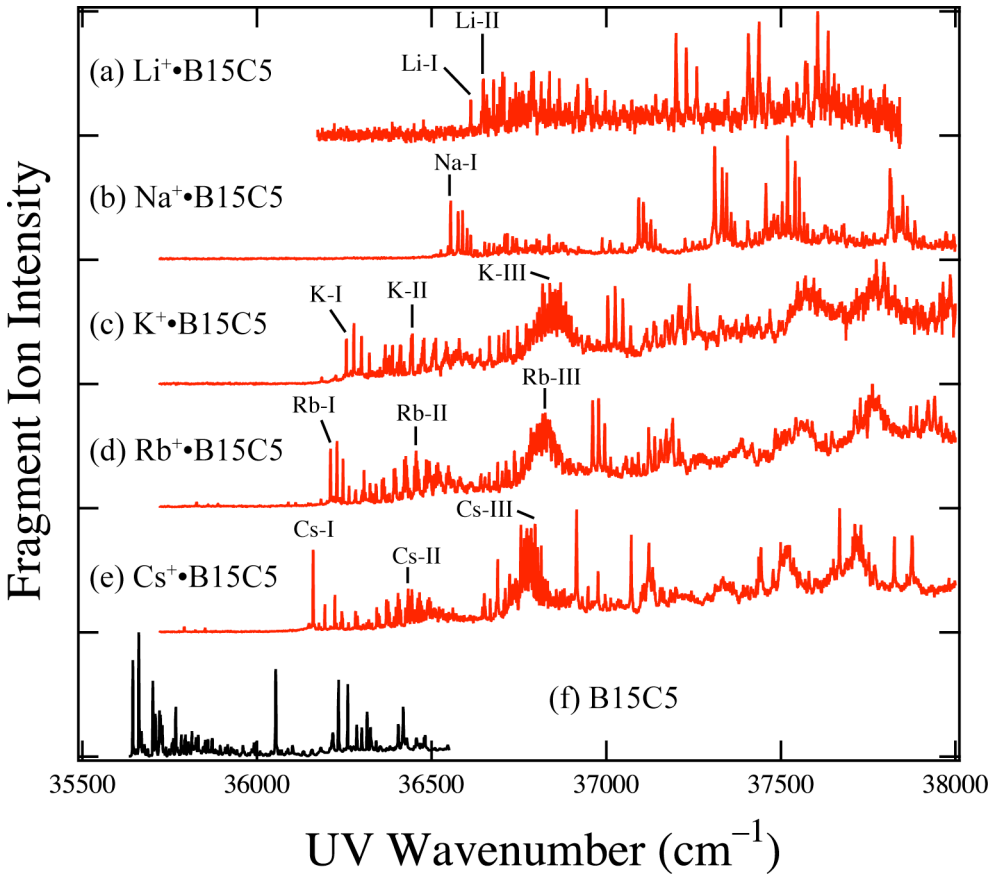

Figure 1. The UVPD spectra of the M^+•B15C5 (M = Li, Na, K, Rb and Cs) complexes with the LIF spectrum of jet cooled B15C5 reported by Zwier and co-workers (Refs. 38 and 39). The temperature of the cooled complex is estimated to be ~10 K.

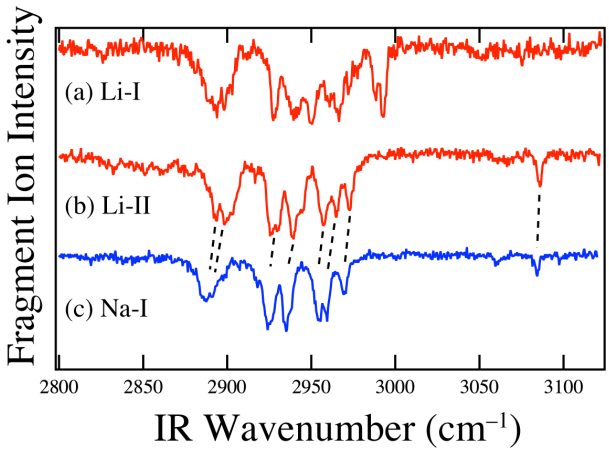

Figure 2. The IR-UV double resonance spectra of the Li^+•B15C5 (a, b) and Na^+•B15C5 (c) complexes in the CH stretching region. These IR spectra are measured by monitoring the intensity of the vibronic bands labeled Li-I, Li-II, and Na-I in Fig. 1.

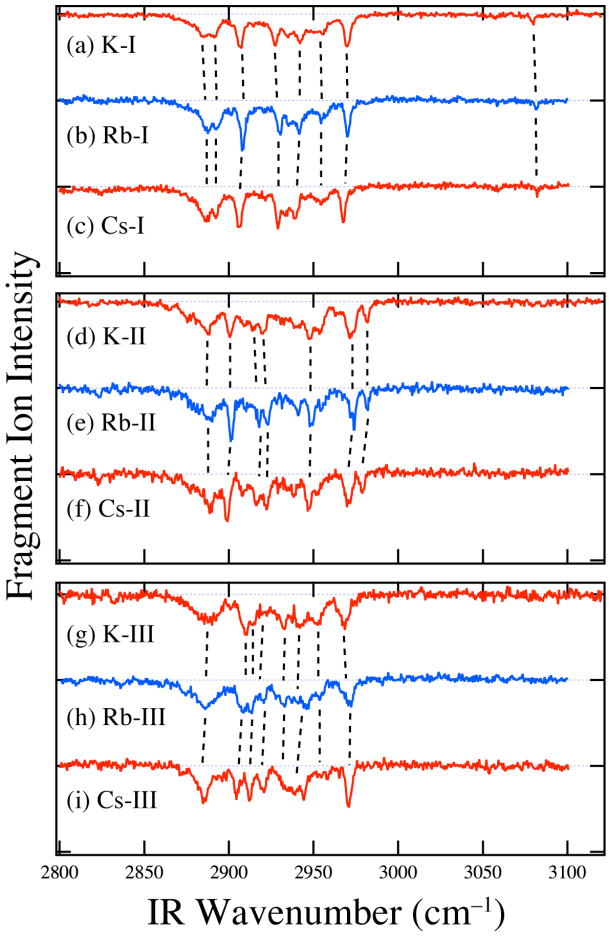

Figure 3. The IR-UV double resonance spectra of the K^+•B15C5, Rb^+•B15C5 and Cs^+•B15C5 complexes in the CH stretching region. These IR spectra are measured by monitoring the intensity of vibronic bands I, II and III in the UVPD spectra of the K^+, Rb^+ and Cs^+ complexes.

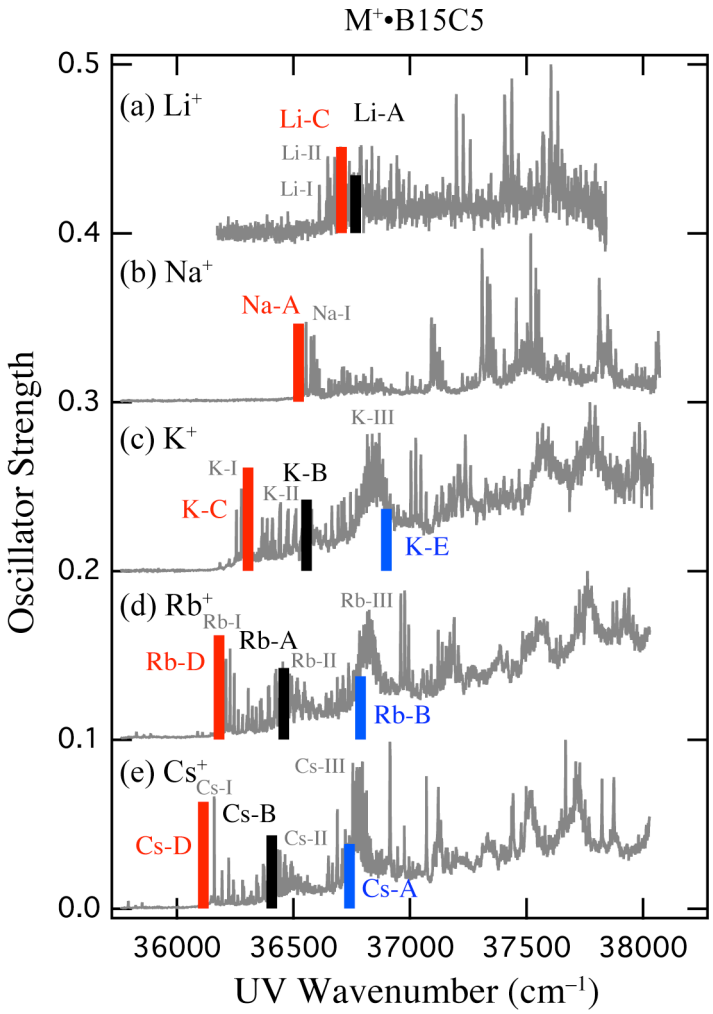

Figure 4. Oscillator strengths of electronic transitions for the M^+•B15C5 (M = Li, Na, K, Rb, Cs) complexes calculated with TD-DFT at the M05-2X/6-31+G(d) level and the Stuttgart RLC potential for Rb and Cs. Calculated transition energies are scaled with a scaling factor of 0.8340 to compare the calculated and experimental spectra. The scaling factor was determined to reproduce the transition energy of the K^+•DB18C6 complex in our previous study (Ref. 31).

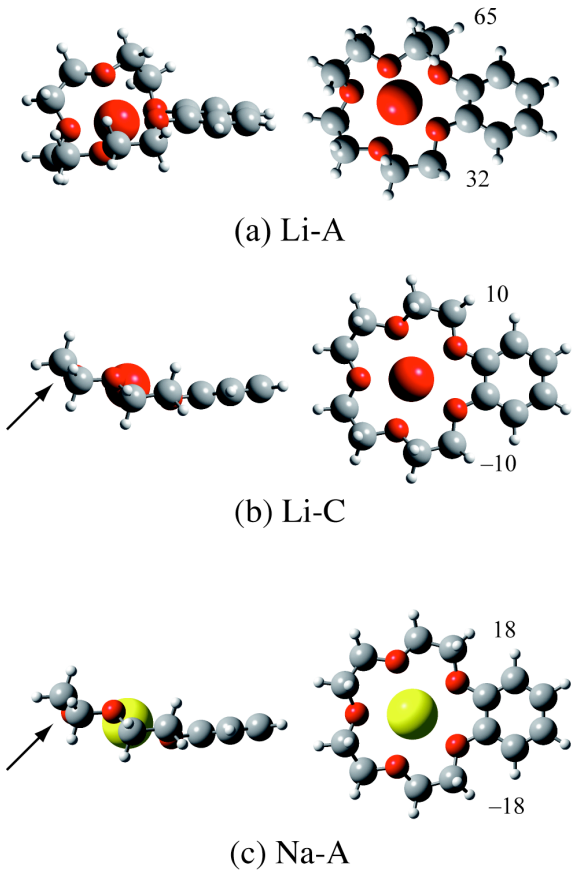

Figure 5. The structure of the (a, b) Li^{+}•B15C5 and (c) Na^{+}•B15C5 complexes optimized at the M05-2X/6-31+G(d) level of theory. The numbers in the figure represent the dihedral angle of C14–O15–C1–C16 and C4–O3–C2–C19 (see Scheme I). The arrows highlight the difference in the conformation from K-C, Rb-D, and Cs-D in Fig. 6.

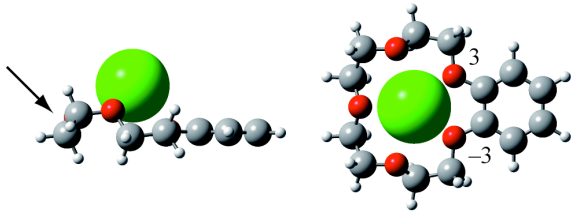

(a) K-C

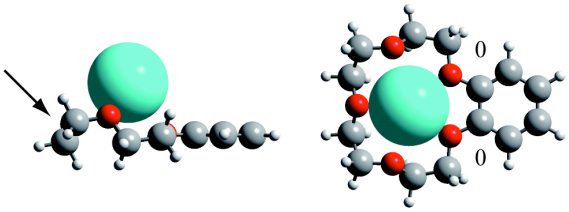

(b) Rb-D

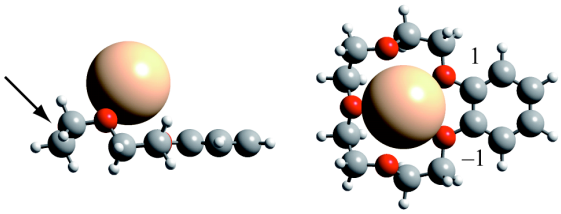

(c) Cs-D

Figure 6. The structure of conformer group I of the K^+•B15C5, Rb^+•B15C5, and Cs^+•B15C5 complexes optimized at the M05-2X/6-31+G(d) level of theory with the Stuttgart RLC potential for Rb and Cs. The numbers in the figure represent the dihedral angle of C14–O15–C1–C16 and C4–O3–C2–C19 (see Scheme I). The arrows highlight the difference in the conformation from Li-C and Na-A in Fig. 5.

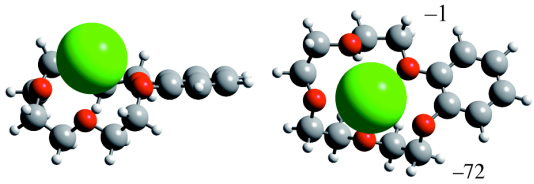

(a) K-B

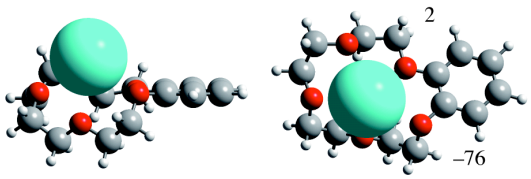

(b) Rb-A

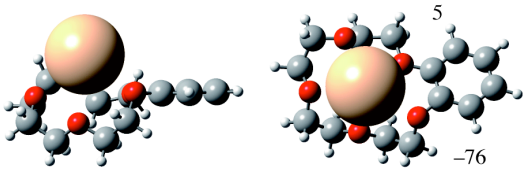

(c) Cs-B

Figure 7. The structure of conformer group II of the K^+•B15C5, Rb^+•B15C5 and Cs^+•B15C5 complexes optimized at the M05-2X/6-31+G(d) level of theory with the Stuttgart RLC potential. The numbers in the figure represent the dihedral angle of C14–O15–C1–C16 and C4–O3–C2–C19 (see Scheme I).

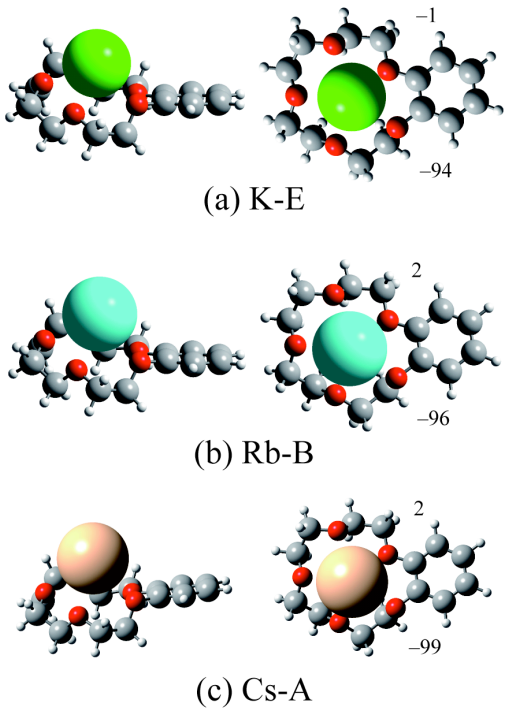

Figure 8. The structure of conformer group III of the K^+•B15C5, Rb^+•B15C5 and Cs^+•B15C5 complexes optimized at the M05-2X/6-31+G(d) level of theory with the Stuttgart RLC potential. The numbers in the figure represent the dihedral angle of C14–O15–C1–C16 and C4–O3–C2–C19 (see Scheme I).

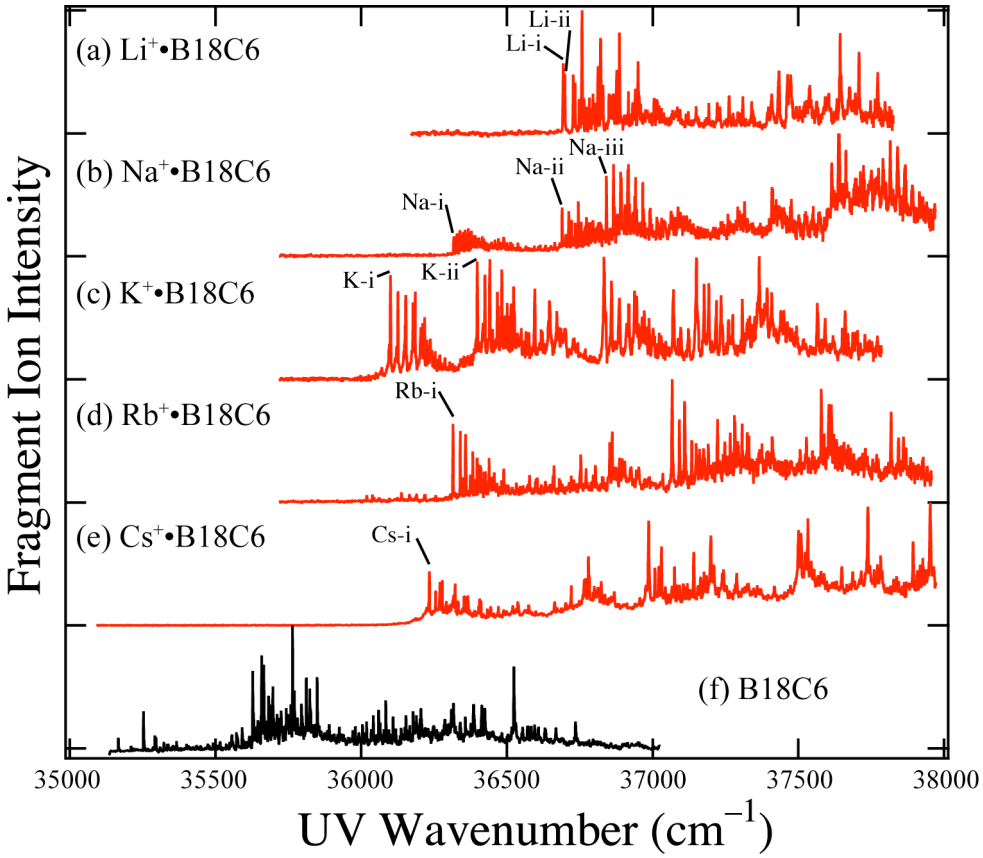

Figure 9. The UVPD spectra of the M^+•B18C6 (M = Li, Na, K, Rb and Cs) complexes with the LIF spectrum of jet cooled B18C6 reported by Ebata and co-workers (Refs. 42 and 43). The temperature of the cooled complex is estimated to be ~10 K.

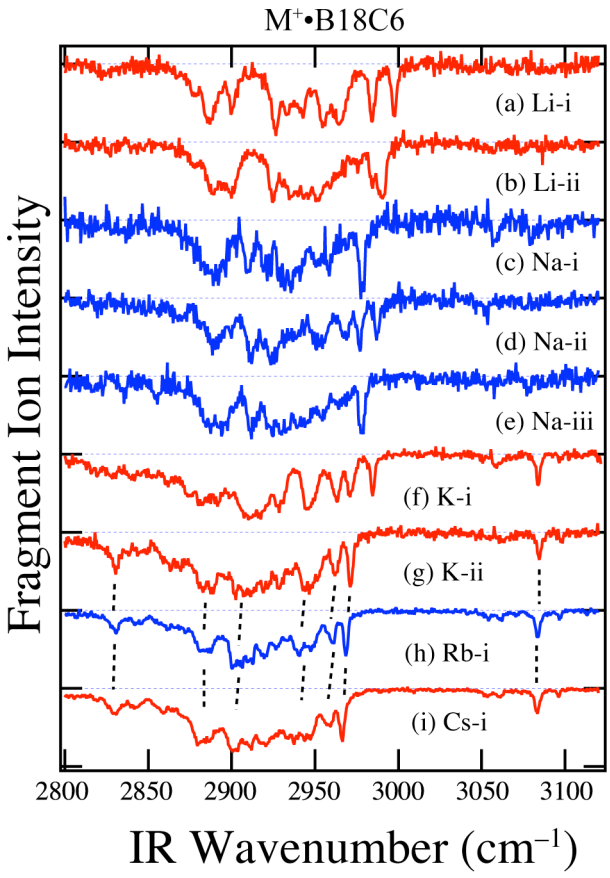

Figure 10. The IR-UV double resonance spectra of the M^+•B18C6 complexes in the CH stretching region.

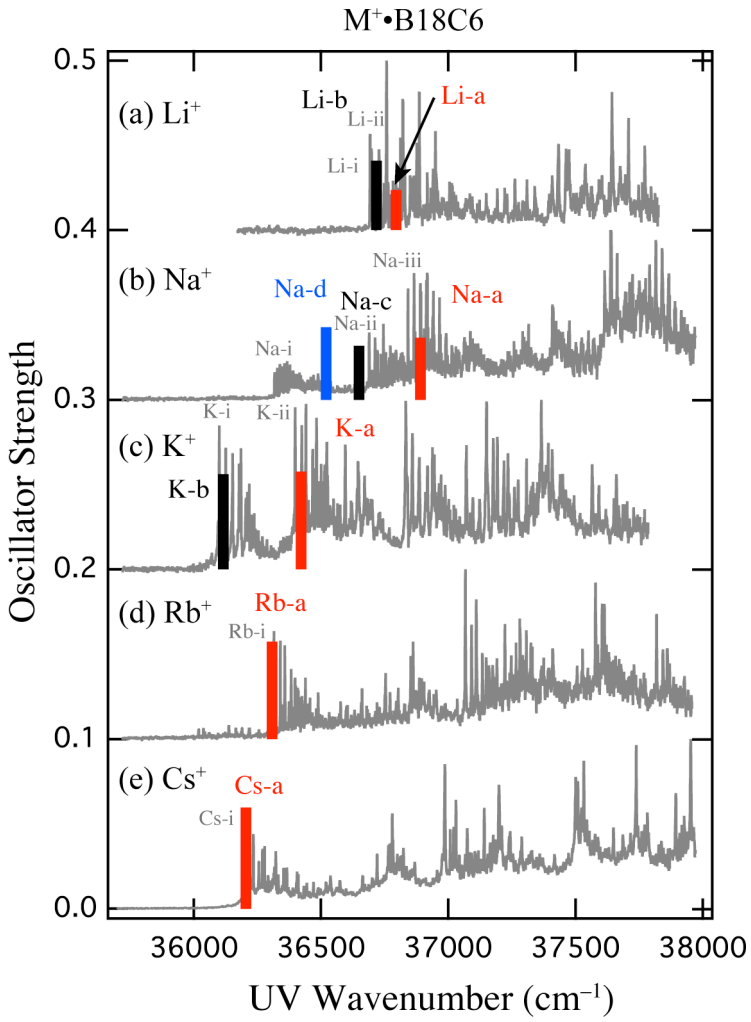

Figure 11. Oscillator strengths of electronic transitions for M^+•B18C6 (M = Li, Na, K, Rb, Cs) calculated with TD-DFT at the M05-2X/6-31+G(d) level and the Stuttgart RLC potential for Rb and Cs. Calculated transition energies are scaled with a scaling factor of 0.8340 to compare the calculated and experimental spectra. The scaling factor was determined so as to reproduce the transition energy of K^+•DB18C6 in our previous study (Ref. 31).

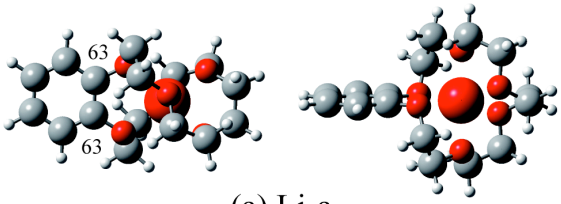

(a) Li-a

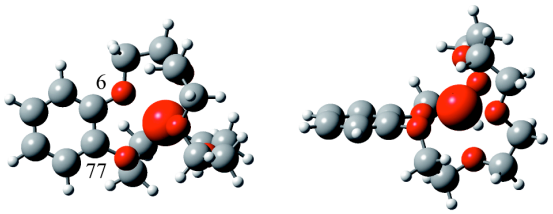

(b) Li-b

Figure 12. The structure of the Li^+•B18C6 complex optimized at the M05-2X/6-31+G(d) level of theory. The numbers in the figure represent the dihedral angle of C17–O18–C1–C19 and C4–O3–C2–C22 (see Scheme I).

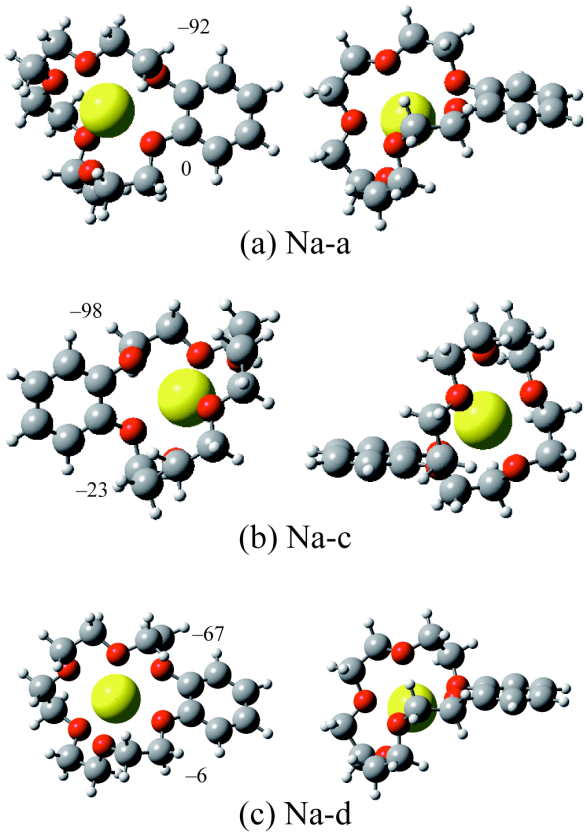

Figure 13. The structure of the Na^{+}•B18C6 complex optimized at the M05-2X/6-31+G(d) level of theory. The numbers in the figure represent the dihedral angle of C17–O18–C1–C19 and C4–O3–C2–C22 (see Scheme I).

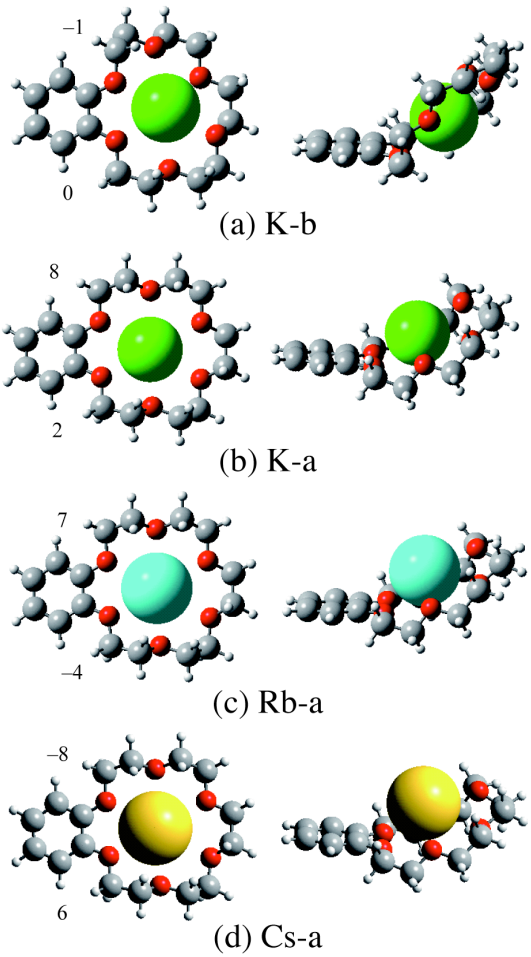

Figure 14. The structure of the (a, b) K^+•B18C6, (c) Rb^+•B18C6 and (d) Cs^+•B18C6 complexes optimized at the M05-2X/6-31+G(d) level of theory with the Stuttgart RLC potential for Rb and Cs atoms. The numbers in the figure represent the dihedral angle of C17–O18–C1–C19 and C4–O3–C2–C22 (see Scheme I).

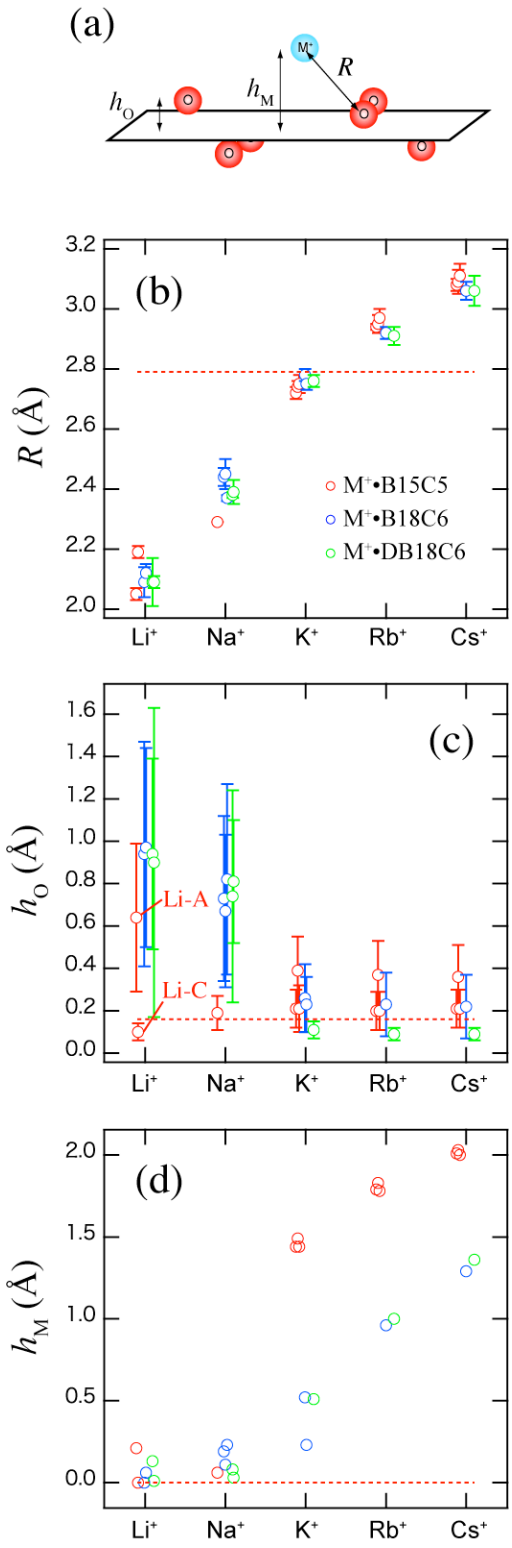

Figure 15. (a) Definition of geometric parameters in the M^+•B15C5, M^+•B18C6 and M^+•DB18C6 complexes. (b) Distance between M^+ and oxygen atoms of crown ethers calculated at the M05-2X/6-31+G(d) level with the Stuttgart RLC potential for Rb and Cs atoms. (c, d) Distance from the mean plane formed by the oxygen atoms of crown ethers to the oxygen atoms (h_O) and to the metal ion (h_M).

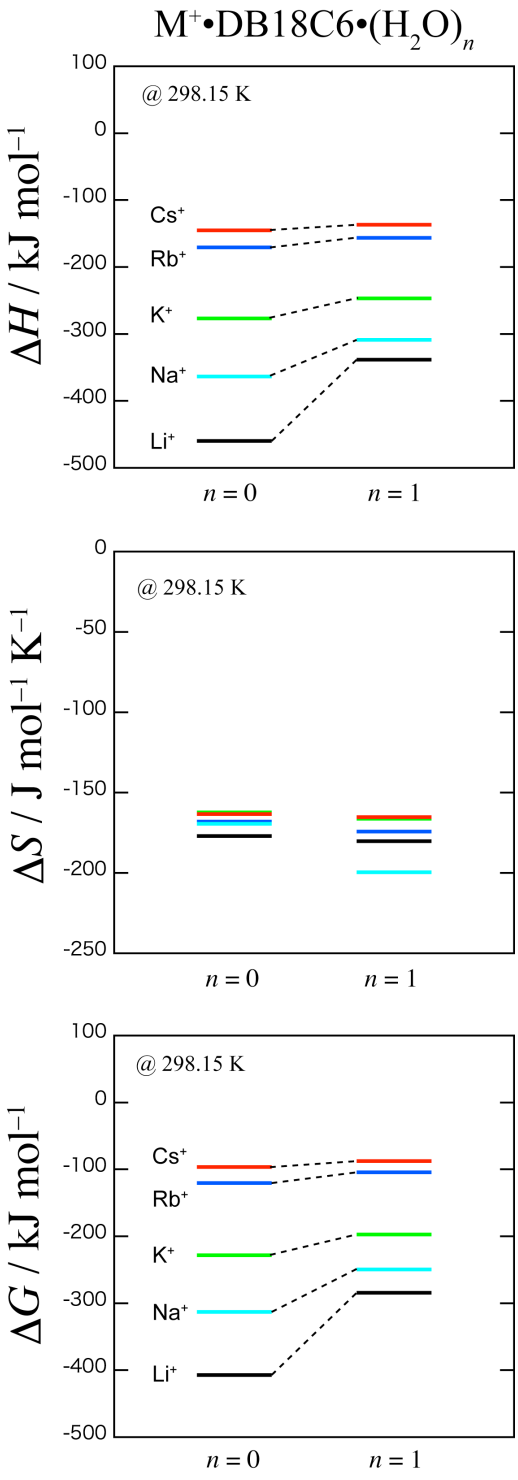

Figure 16. The ΔH, ΔS and ΔG values for the complex formation between $M^+•(H_2O)_n$ and DB18C6 at 298.15 K and 1.0 atom. These data are calculated on the basis of the most stable conformers of the M^+•DB18C6 complexes (Ref. 31). The results of B18C6 and B15C5 are displayed in Figs. 26S and 27S in the Supporting Information.

Table 1. The number of conformers found experimentally for the M^+•B15C5, M^+•B18C6 and M^+•DB18C6 complexes under the cold conditions of our ion trap.

M	M^+•B15C5	M^+•B18C6	M^+•DB18C6[a]
Li	2	2	2
Na	1	3	2
K	3	2	1
Rb	3	1	1
Cs	3	1	1
(monomer)	3[b]	4[c]	2[c]

[a] Ref. 31
[b] Ref. 38
[c] Refs. 42 and 43

TOC Figure